Materials and Structures (2017) 50:132
DOI 10.1617/s11527-017-1006-x

ORIGINAL ARTICLE

Drying and carbonation shrinkage of cement paste containing alkalis

Hailong Ye · Aleksandra Radlińska · Juliana Neves

Received: 8 March 2016 / Accepted: 30 January 2017 / Published online: 6 February 2017

Abstract In this work, shrinkage performance of ordinary portland cement (OPC) paste containing various alkali salts was characterized at two drying conditions, namely: nitrogen gas and air. The results show that incorporation of alkalis dramatically increases shrinkage magnitude, but reduces shrinkage kinetics of OPC, regardless of source and type of alkalis (e.g. Na^+ or K^+). The amount of alkalis bound in the solid hydrated phases, rather than the free alkalis remaining in the pore solution, is crucial in controlling the shrinkage performance of OPC. It is suggested that the alkali enrichment in OPC increases the visco-elastic/visco-plastic compliance (reduce creep modulus) of its solid skeleton under drying-induced internal stresses. This phenomenon is likely to be attributed to the alkalis binding in calcium–silicate–hydrate (C–S–H), which promotes the packing of C–S–H nanoparticles. Carbonation results in shrinkage (i.e. carbonation shrinkage) in plain OPC, but expansion in OPC with alkali enrichment. The overall volume change of OPC due to carbonation may be a result of competition between dissolution-induced shrinkage and crystallization-induced expansion.

H. Ye (✉) · A. Radlińska · J. Neves
Department of Civil and Environmental Engineering, The Pennsylvania State University, 3127 Research Drive, State College, PA 16801, USA
e-mail: huy131@psu.edu

Keywords Cement · Alkalis · Carbonation shrinkage · Drying shrinkage · Shrinkage mechanisms · Calcium–silicate–hydrate

1 Introduction

Given the high environmental impacts related to production of ordinary portland cement (OPC), increasing efforts are being made towards alternative binder systems, including OPC blended with supplementary cementitious materials (SCMs) and alkali-activated materials [1, 2]. For these alternative binders, alkalis (e.g. sodium or potassium), either from SCMs or alkaline activators, become incorporated into the matrix to much higher degree than in plain OPC system. The addition of alkalis has dramatic impact on volumetric stability of hardened cement paste, including larger autogenous and drying shrinkage [3–8], and enhanced tendency to micro-cracking [7, 9, 10]. On the other hand, the addition of alkalis in OPC promotes carbonation, increasing carbonation depth and mass gains, as compared to the plain system [11]. The addition of alkalis salts increases the alkalinity of pore solution, which would increase the carbonation rate of cement [12]. However, it remains unknown whether the enhanced carbonation of OPC containing alkalis would result in high carbonation shrinkage in the atmosphere, which would further degrade its volumetric properties.

Carbonation shrinkage of cement can potentially result in pore coarsening, loss of strength cohesion, and micro-cracking, which is detrimental to the long-term performance of concrete.

When hardened cement or concrete are exposed to the atmospheric condition, drying and carbonation occur simultaneously, resulting in combined volume change, compositional and phase (hydrates and pore solution chemistry) evolution. Some of the published experimental data on drying shrinkage actually include the effects of carbonation [13]. However, the mechanisms of drying and carbonation shrinkage are intrinsically different. Drying shrinkage is the volume change (including reversible and irreversible components) of hardened cement paste due to moisture loss, while carbonation shrinkage is the irreversible volume change due to chemical reaction with the carbon dioxide (CO_2) in the atmosphere. The magnitudes of drying and carbonation shrinkage of cement paste are dependent on the relative humidity (RH), ambient temperature, curing condition, and specimen size [14]. In addition, carbonation shrinkage of cement varies with CO_2 concentration and sequence of drying and carbonation [14]. Therefore, in order to illustrate the effects of carbonation on the volumetric stability of realistic OPC containing alkalis, it is important to study the shrinkage behaviors at both inert gaseous and atmospheric conditions.

Although the phenomenon of carbonation-induced volume change in cement has been known for decades, the mechanisms are still unclear, since carbonation of cement paste should theoretically result in an increase in unit cell volume, whether the carbonated product is calcite, aragonite, or vaterite. Several mechanisms for the carbonation shrinkage of OPC have been proposed. For example, Powers [15] attributed carbonation shrinkage of cement to a temporary increase in the compressibility of solid skeleton due to the reduction of crystallization stress during dissolution of portlandite crystals. Powers argued that the precipitation of calcite (or aragonite, or vaterite) in the pores does not exert crystallization pressure on the solid skeleton [15]. Nevertheless, a recent study shows that the dissolution of portlandite is coupled with the precipitation of thick islands of calcite that appear oriented on the substrate [16]. On the other hand, some researchers [17, 18] claimed that decalcification of calcium–silicate–hydrate (C–S–H) is the primary mechanism responsible for carbonation shrinkage of cement. It was postulated that the double-chain silicate anion structures in C–S–H are decomposed, shrink, and polymerize to silica-gel-like structure, as the Ca ions progressively dissolve from the Ca–O layer in C–S–H [18]. Given that either the precipitation of portlandite or composition and structure of C–S–H are altered by the addition of alkalis in OPC [19–21], investigating the carbonation shrinkage of alkali-enriched OPC system would shed some lights on the underlying mechanisms of this reaction.

On the other hand, although it was acknowledged that alkali-enrichment increases the magnitude of drying shrinkage in OPC, the scientific reasoning behind the enlarged shrinkage remains unclear. Some researchers attributed the enlarged shrinkage of OPC containing alkalis to the increased effective capillary stress and degraded bulk modulus (due to enlarged porosity) [3]. However, others argued that the enlarged shrinkage originates from the increased disjoining pressure due to the enlarged ionic concentration in the pore solution [4]. A recent study showed that the alkali cation can potentially reduce the stacking regularity of C–S–H layers and make C–S–H easy to collapse and redistribute upon drying, resulting in enhanced irreversible shrinkage [22–24]. However, none of the previous studies has ever provided a detailed explanation of unique shrinkage performance of alkali-enriched OPC from a microstructural viewpoint.

To fill the aforementioned knowledge gaps, this study investigated the drying and carbonation shrinkage of OPC containing various alkali salts and aimed to provide a thorough understanding of the effects of alkalis on the volumetric properties of cement-based materials.

2 Experiments

2.1 Materials and specimens

Four types of cement paste mixtures were investigated by mixing OPC with different solutions. The cement used was ASTM Type I with a specific gravity of 3.15 and total equivalent alkalis content ($Na_2O + 0.658K_2O$) of 0.89. The main compounds in the OPC were 46.80% C_3S, 20.54% C_2S, 6.46% C_3A, and 12.45% C_4AF by mass. The solutions were prepared by dissolving NaOH pellets, NaCl powders, or KOH pellets in distilled water, to reach the targeted

Table 1 Mix proportion for OPC paste containing various alkalis

Mixture ID	Solution	Initial porosity
OPC (control)	Distilled H_2O	56.52%
OPC/NaOH	2 M NaOH	
OPC/NaCl	2 M NaCl	
OPC/KOH	2 M KOH	

concentration shown in Table 1. The four mixtures were designed to have the same initial porosity (i.e. ratio between the volume of mixing solution to the total volume of mixing solution and cement) of 56.52%, which is equivalent to a water-to-cement ratio of 0.41 for plain OPC. The paste was mixed according to ASTM C305-12, and was cast into a non-standardized prism molds with dimensions of 12.7 mm × 12.7 mm × 139.7 mm (½ inch × ½ inch × 5½ inches). The use of smaller geometry enabled the samples to reach equilibrium with the environment in a much shorter time. All paste samples were cured in the moist room (100%RH, 23 ± 0.5 °C) for 24 h before demolding.

2.2 Length and mass changes

After demolding, samples were placed in two drying environments:

Nitrogen gas condition: Vena VC-10 environmental chambers were programmed at 50% RH and 23 °C. To prevent carbonation of samples, dry nitrogen (N_2) was purged into chambers continuously and the concentration of CO_2 was periodically checked to be consistently 0 ppm.

Atmospheric condition: A walk-in environmental chamber, which was maintained at 50 ± 4% RH and 23 ± 0.5 °C, was used. The concentration of CO_2 in that room was measured to be about 400 ppm.

The changes in length and mass of all samples during drying at these two conditions were recorded utilizing a modified digital comparator with a measuring accuracy of 0.0001 inches, and a high precision balance with an accuracy of 0.01 g.

2.3 X-ray diffraction (XRD)

In order to illustrate the effects of carbonation on phase assemblage of OPC, after drying in nitrogen and atmospheric conditions for about 115*d*, paste samples were collected for XRD analysis. Considering that the extent of carbonation for carbonated samples is depth-dependent, the entire bulk of paste samples used for shrinkage measurement were analyzed to provide the overall information. The same batch of cement paste was also cast in a series of sealed plastic vials to investigate the effects of alkali salts on the phase evolution in OPC at early ages, namely, 1*d*, 7*d*, and 28*d*.

All samples were first immersed in isopropyl alcohol for two weeks and then vacuum dried for one week (i.e. solvent-exchange and vacuum-drying). Afterwards, they were crushed and milled for about 15 min and front-filled into a zero-background plate. XRD data was collected using a PANalytical Empyrean diffractometer in a conventional Bragg–Brentano θ–2θ configuration. CuKα X-ray (λ = 1.5418 Å) was generated using 40 mA and 45 kV operating conditions. Incident beam Soller slits of 0.04 radians were used, and the incident divergence and anti-scatter slits were fixed at 0.25° and 0.5°, respectively. The samples were scanned continuously between 5° and 45° 2θ under these conditions.

2.4 Scanning electron microscopy (ESEM/EDS)

FEI Quanta 200 equipped with X-ray microanalysis was adopted to investigate the composition of hydrated phases in OPC samples. The samples which were sealed in plastic vials for 28*d* were first solvent-exchanged and vacuum-dried, then impregnated with a low viscosity epoxy in desiccators, the hardened epoxy at the surface was polished off, and the specimens were polished down to 1 μm. Specimens were carbon coated prior to SEM/EDS analysis. More than 50 microanalysis data points were collected randomly across the hydrated matrix for each sample.

2.5 Mercury intrusion porosimetry (MIP)

The MIP was applied to samples that were dried at nitrogen and atmospheric conditions for 115*d*. The pore entry diameters ranging from 360 to 0.003 μm in samples can be measured using MIP. Prior to MIP, all samples were solvent exchanged and vacuum dried using the same procedure explained in Sect. 2.3.

2.6 Inductively coupled plasma emission spectrometry (ICP-AES)

The pore solutions of all mixtures after casting for 1*d* were extracted using a high-pressure steel die [25]. The extracted pore solutions were filtered through a 0.2 μm Millipore filter immediately after extraction. The pH of the pore solutions was determined using acid titration and phenolphthalein as the indicator, immediately after filtration. In addition, the extracted pore solutions were diluted 10 times with 2% HNO_3 solution to avoid precipitates, then used to measure the concentration of Ca^{2+}, Na^{+}, K^{+}, and SO_4^{2-} ions using ICP-AES.

3 Results and discussion

3.1 XRD

Figure 1 shows the XRD patterns of OPC containing various alkali salts cured for 1*d*, 7*d*, and 28*d*. It can be seen that in comparison to plain OPC, the addition of NaOH or KOH depresses the formation of AFt and carbonate-AFm phases (i.e. ettringite, monocarbonate, and hemicarbonate), but promotes the formation of sulfate-AFm (i.e. monosulfate). In addition, the portlandite detected in OPC blended with NaOH or KOH shows a decreased diffraction intensity and more diffusive shape, indicating a modification of crystallinity, morphology, size, or amount of portlandite, as compared to that in the plain system. On the other hand, the addition of NaCl generates the Friedel's salts but depresses the formation of carbonate-AFm, which may be attributed to the more stable nature of Friedel's salts [26]. However, the addition of NaCl preserves the existence of AFt, suggesting that AFt is destabilized at the high pH environment. This argument is further evidenced by the high sulfate (SO_4^{2-}) concentration in the pore solution of OPC blended with NaOH and KOH, as shown in Table 2.

3.2 SEM/EDS

Figure 2 shows the atomic relationship, including Al/Ca and (Na + K)/Ca ratios versus Si/Ca ratio, in the solid hydrated phases of OPC. It should be noted that due to the large interaction volume between electron and specimen, each individual EDS datum point represents the composition of mixed hydrated phases. The cluster in Fig. 2a is primarily a combined composition of C–S–H, portlandite, and AFm or AFt phases. It can be seen that, in comparison to plain OPC, the OPC blended with NaOH or KOH shows a lower overall Si/Ca ratio, which may be attributed to a high proportion of portlandite formation. According to previous studies [27], the addition of alkali hydroxide seems to accelerate the precipitation of portlandite in the cement at an early age due to the increased pH, which principally requires less amount of Ca^{2+} to reach the supersaturation with respect to portlandite. On the other hand, although NaCl does not dramatically change the composition of C–S–H clusters, as compared to plain OPC, it introduces several points with high Al/Ca or Si/Ca ratio, which may correspond to the formation of chloride-bearing phases (e.g. Friedel' or Kuzel's salts).

The (Na + K)/Ca ratio versus Si/Ca ratio plot (see Fig. 2b) shows a strong linear relationship, as the amount of bound alkali tends to increase with the increasing silicate content, regardless of the type and source. This observation evidences the alkali binding into the silicate structure and/or onto the surface of C–S–H. In C–S–H, the alkali cations (Na^{+}, K^{+}) can compete with Ca^{2+} on compensating the negative surface charge of silicate chains due to de-protonation of −SiOH to –SiO– sites. Furthermore, the alkalis can progressively incorporate into the atomic structure of C–S–H, resulting in shortening of silicate chain length [28] and creating non-bridging oxygen. As such, it is not surprising to observe this strong linear relationship. However, it should be noted that differentiating the alkali binding sites either in the nanostructure (interlayer) or at the surface of C–S–H is challenging via current techniques [22].

Moreover, it can be seen from Fig. 2b that the amount of bound alkalis in hydrates of OPC is strongly dependent on the type and source of alkalis. For example, the amount of alkalis bound in solid phases is larger when OPC was blended with NaOH, as compared to that blended with NaCl, although the Na concentration remaining in the pore solution is higher for the latter (see Table 2). The different amount of alkalis bound on hydrates between NaOH- and NaCl-mixed OPC can be attributed to the difference in pH of pore solution. The higher pH can render in a stronger de-protonation of silicate, which results in higher negative surface charge and adsorbs more

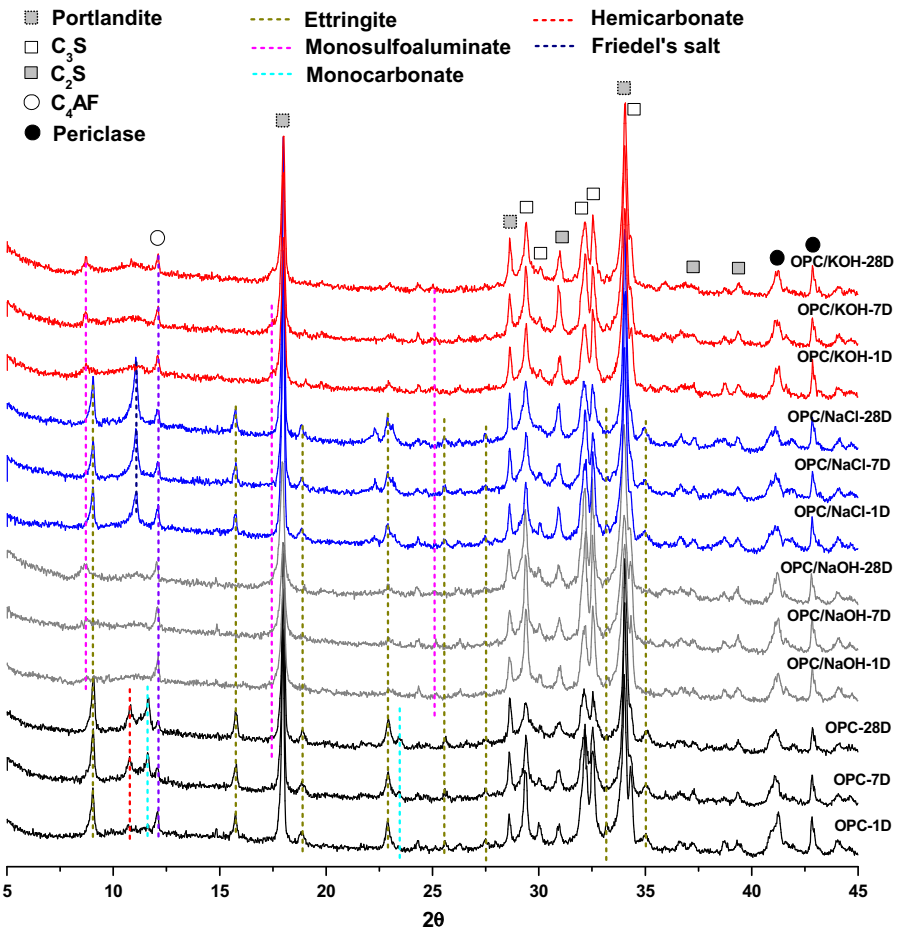

Fig. 1 XRD patterns of OPC containing various alkalis at 1*d*, 7*d*, and 28*d*

Table 2 Pore solution composition of OPC containing various alkalis

Mixture ID	Na^+ (mM)	K^+ (mM)	Ca^{2+} (mM)	SO_4^{2-} (mM)	pH
OPC (control)	123.17	285.47	4.72	82.90	13.61
OPC/NaOH	1597.71	324.92	1.72	525.65	14.02
OPC/NaCl	2126.02	392.34	4.22	103.78	13.41
OPC/KOH	103.90	1505.62	1.45	313.72	14.04

charge compensating cations such as Na^+ and K^+. The detailed explanation on the interaction between C–S–H and alkalis can be found in the work by Lothenbach et al. [29].

3.3 Drying shrinkage

Figure 3 shows the length and mass changes, as well as the correlation between length and mass changes, for OPC containing various alkalis dried under both nitrogen and atmospheric conditions. When dried in nitrogen condition, the magnitude of drying shrinkage is dramatically increased (up to 6–7 times higher than that of plain OPC) as a result of alkali salts additives. Additionally, inclusion of alkalis generally reduces the moisture loss of OPC when conditioned at the same RH. In addition, the slope of shrinkage per moisture loss becomes much steeper for OPC containing alkalis, in comparison to plain system (see Fig. 3c).

Figure 4 shows the kinetics of drying shrinkage and mass change, as well as the correlation between shrinkage rate and mass changes for samples dried in nitrogen. It can be seen that the shrinkage development of OPC blended with alkalis (especially with

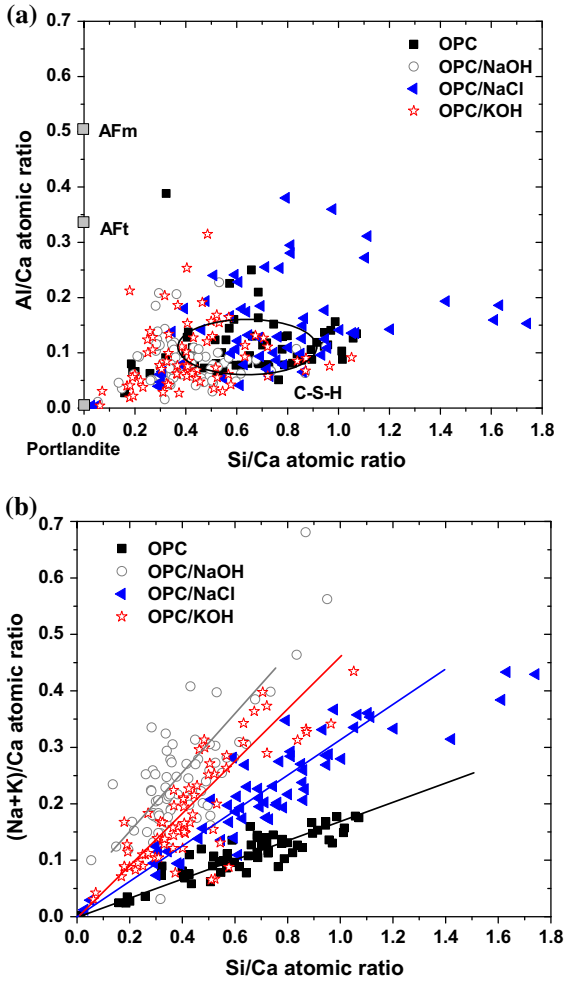

Fig. 2 Atomic relationship in the solid hydrated phases of OPC at 28*d* **a** Si/Ca ratio versus Al/Ca ratio; **b** (Na + K)/Ca ratio versus Si/Ca ratio (the *lines* are merely for visional guide)

NaOH or KOH) shows much slower kinetics and exhibits a characteristic visco-elastic/visco-plastic (creep) deformation. That is to say, as shown in Fig. 4c, the shrinkage rates of alkali-rich OPC can be considerably high despite the mass changes being almost constant (This indicates a constant shrinkage driving force as will be elaborated in the following discussions). This is an indication of creep component in the drying shrinkage of OPC under drying-induced internal stresses.

Before understanding the causes of the enlarged shrinkage magnitude and visco-elastic/visco-plastic

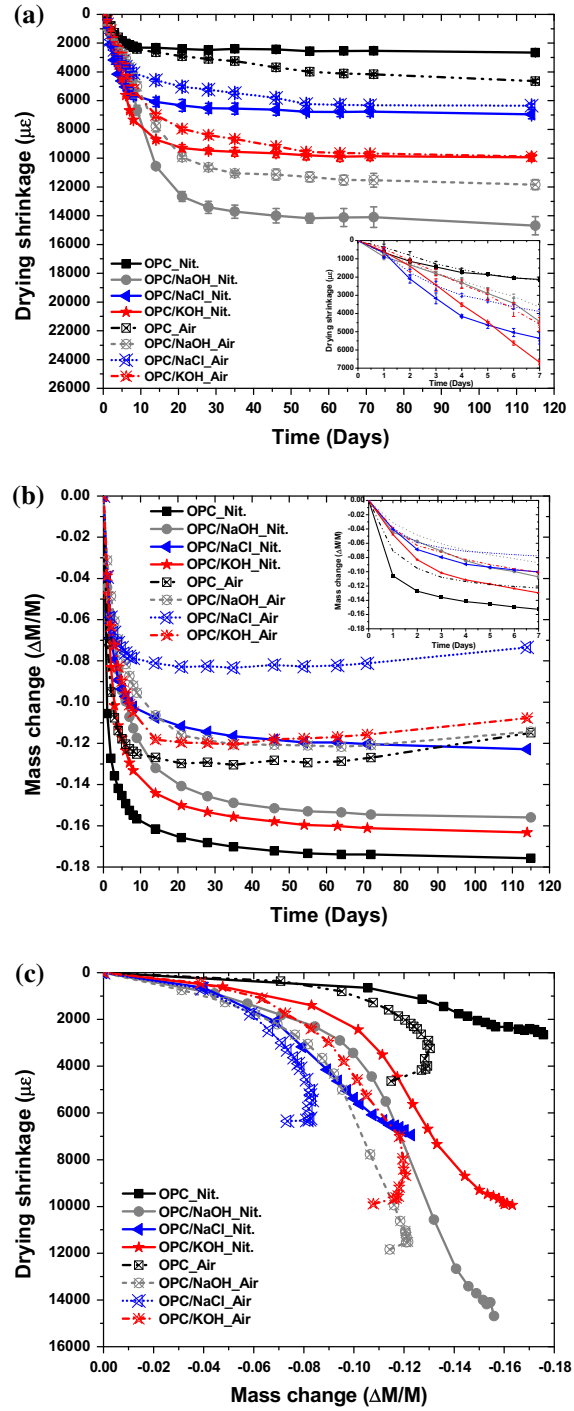

Fig. 3 **a** Time-dependent shrinkage development of four OPC paste with various alkalis. **b** Time-dependent mass change. **c** Correlation of shrinkage and mass change

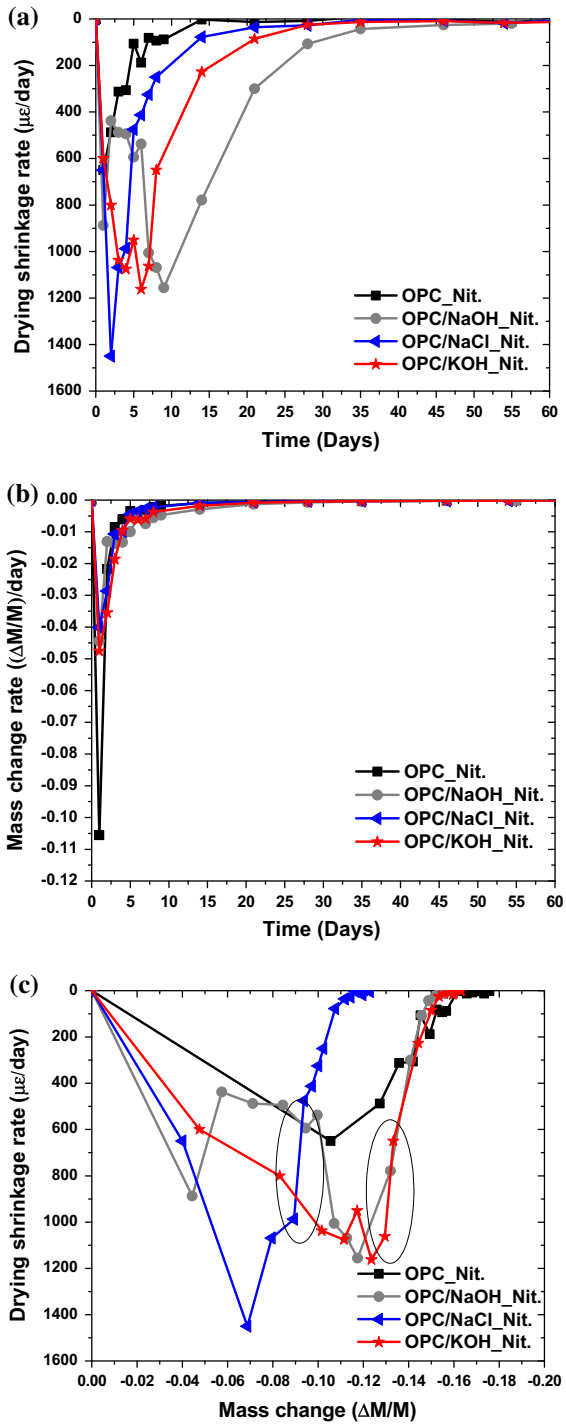

Fig. 4 **a** Time-dependent evolution of drying shrinkage rate. **b** Time-dependent evolution of moisture loss rate (only shows the first 60*d* data). **c** Shrinkage rates as a function of mass change

deformation characteristics in OPC with alkali enrichment, the basic shrinkage mechanisms at high RH for cementitious materials need to be revisited. At high pH, capillary pressure and/or disjoining pressure have been generally regarded by previous researchers as the main shrinkage driving force [30–32].

According to capillary pressure theory, the measured relative humidity (RH) at equilibrium condition in an unsaturated pore system is influenced by the formation of capillary menisci due to drying, as well as the water activity of the pore solution due to salt effects. The measured RH in cementitious materials can be expressed as [32]:

$$\mathrm{RH} = \mathrm{RH_S RH_K} = x_{\mathrm{w}} \exp\left(\frac{p_{\mathrm{l}} M_{\mathrm{l}}}{\rho_{\mathrm{l}} RT}\right) \tag{1}$$

In which the *RH* is the measured relative humidity (%); RH_S is the contribution to the RH due to salts in the pore fluid, which can be approximated as the molar fraction of water in pore solution, x_w, for ideal solution using Raoult's law (%); It should be noted that Raoult's law is only strictly applicable at the dilute limit as a means to approximate the reduction in pore water chemical potential due to the presence of dissolved species. As a cementitious material dries and the ionic concentrations in the pore solution increase, the validity of Raoult's law may be questionable [33]. RH_K is the contribution to the RH due to formation of liquid–vapor meniscus, which can be expressed using Kelvin equation (%); p_l is the liquid pressure (Pa); ρ_{l} is the density of pore liquid (kg/m^3), M_l is the molar mass of liquid (kg/mol), $R = 8.314$ [J/(mol K)] is the universal gas constant, T is the temperature (K).

Due to the formation of menisci in the pores, there exist a difference between the gas pressure above the meniscus and the pressure inside the liquid, which is called capillary pressure. The capillary pressure in a cylindrical shape pore can be calculated using the Young–Laplace equation:

$$p_c = p_g - p_l = -\frac{2\gamma \cos\theta}{r_c - t} \tag{2}$$

where p_c is the capillary pressure (Pa), p_g is the gas pressure (Pa), p_l is the liquid pressure (Pa), r_c is the capillary radius at the position of meniscus (also

named as the Kelvin radius) (m), γ is the surface tension between pore water and vapor (N/m), θ is the contact angle denoting the hydrophilicity of the pore wall (°), and t is the thickness of an adsorbed layer (m), which is a function of RH [34, 35]. Since the liquid pressure excesses significantly that of atmospheric pressure during drying (i.e. $\|p_l\| \gg \|p_g\|$), the gas pressure is eliminated and $p_l \approx p_c$. Therefore, combining the Eqs. (1) and (2), enable the calculation of Kelvin radius as:

$$r_c = -\frac{2\gamma \cos\theta M_l}{\ln\left(\frac{RH}{x_w}\right)\rho_l RT} + t \tag{3}$$

The Kelvin radius is also the radius of the largest capillary pore filled with pore fluid at equilibrium condition. All surface pores whose radii are smaller than the Kelvin radius are completely filled with water, whereas larger surface pores are dried and only contain a layer of adsorbed water with a thickness of t.

Since only the pores which are saturated with capillary water can contribute to the formation of capillary pressure, the *effective capillary pressure* can be approximated by multiplying the capillary pressures p_c with the degree of saturation S_w, i.e. $S_w p_c$ [36–38]. It should be noted that the S_w is basically an approximation of the Bishop parameter χ (representing the contact area between liquid and solid) in unsaturated poromechanics. Therefore, the linear shrinkage strain resulting from the internal capillary pressure for isotropic elastic materials can be calculated using Mackenzie equation [37] modified by Bentz [36] to include saturation:

$$\varepsilon_{cap} = -\frac{S_w p_c}{3}\left(\frac{1}{K_b} - \frac{1}{K_s}\right) \tag{4}$$

In which ε_{cap} is the capillary pressure-driven linear shrinkage strain, K_b is the drain bulk modulus of the whole porous body (Pa), K_s is the bulk modulus of the solid skeleton (Pa). Recently, Vlahinić et al. [39] proposed another approach to model the volumetric deformation in a porous, linearly elastic body by considering that the bulk modulus of the solids changes with drying. It should be noted that both the models proposed by Bentz and Vlahinić et al. are only strictly applicable to elastic porous materials, and the direct implementation significantly underestimates the shrinkage of plain OPC.

According to Eq. (4), the high shrinkage of OPC containing alkalis can originate from the increased magnitude of $S_w p_c$ and/or degraded K_b. According to the Eq. (1), the reduction of water activity due to alkali enrichments decreases the magnitude of capillary pressure at a given RH [32, 40]. However, the reduction of water activity increases the Kelvin radius when equilibrated at the same RH, which would increase the degree of saturation when the pore structure is kept unaltered [3]. Therefore, the effective capillary pressure can be decreased or increased depending on the competition between S_w and p_c, although experimental findings support that the effective capillary pressure increases due to alkali enrichment [3]. Additionally, the increase of effective capillary pressure can originate from the refinement of pore structure due to alkali enrichment. As shown in Fig. 5, the addition of alkalis tends to refine the pore structure, especially for sodium-bearing salts. As mentioned before, the degree of saturation tends to increase with a finer pore structure since larger numbers of pores are smaller than Kelvin radius in size and saturated at equilibrium condition, as compared to a coarser pore system.

However, neither the increased effective capillary pressure, nor modified bulk modulus can fully explain the visco-elastic/visco-plastic shrinkage characteristics and the reduced shrinkage kinetics of alkali-enriched OPC system. Any isotropic elasticity-based shrinkage models are therefore not valid in term of explaining or predicting the shrinkage performance of alkali-rich cementitious systems [23].

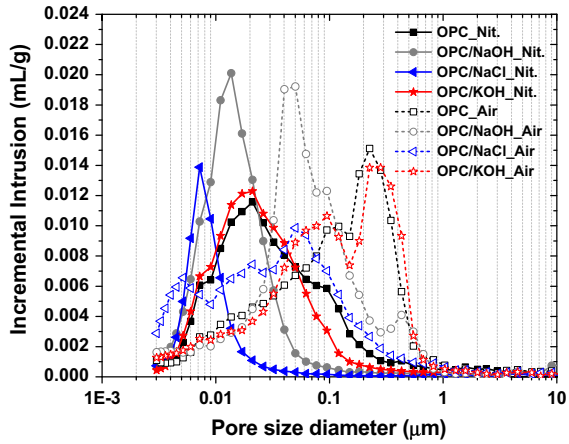

Fig. 5 Pore entry size distribution of OPC containing various alkalis dried at nitrogen and atmospheric condition

The characteristic visco-elastic/visco-plastic deformation of OPC containing alkalis can be attributed to (1) time-dependent shrinkage driving force; (2) visco-elastic/visco-plastic response of solid skeleton under drying-induced internal stresses.

As illustrated in Fig. 4a, b, the kinetics of drying among various OPC systems are similar after drying for 1 day, while the kinetics of shrinkage are considerably different before one month of drying. In addition, as shown in Fig. 4c, the shrinkage rates of OPC with alkali-enrichment are considerably high, despite the moisture loss being almost constant (it corresponds to the almost constant degree of saturation). These observations imply that the alkali-enriched OPC systems undergo extensive visco-elastic/visco-plastic deformation (e.g. creep). It then suggests that the alkali enrichment induces little changes in the time-dependent shrinkage driving force, but considerably increases the visco-elastic/visco-plastic compliance (i.e. decrease creep modulus) of the solid skeleton under drying-induced internal stresses. These results indicate that one cannot model the shrinkage development of cementitious materials merely in term of current mass loss or current RH. Instead, modeling the visco-elastic/visco-plastic behavior of the solid skeleton under internal stresses must be paid considerable attention.

By comparing Fig. 2b with Figs. 3a and 4a, it is found that the shrinkage magnitude tends to increase and the shrinkage kinetics tends to decrease, with the increasing amount of alkalis bound in the solid hydrated phases of OPC. The enhanced alkali binding in the solid skeleton of OPC can be related to the increased visco-elastic/visco-plastic compliance. The visco-elastic/visco-plastic deformation of cement paste is typically attributed to the microstructural rearrangement and reorganization of C–S–H as a result of denser nanoparticles packing [41, 42]. As such, this study suggests that alkali cation may play an important role in facilitating the reorganization and redistribution process of C–S–H nanoparticles upon drying [22]. As mentioned before, the surfaces of C–S–H due to de-protonation of –SiOH to –SiO– sites are negatively charged. The positively charged alkalis

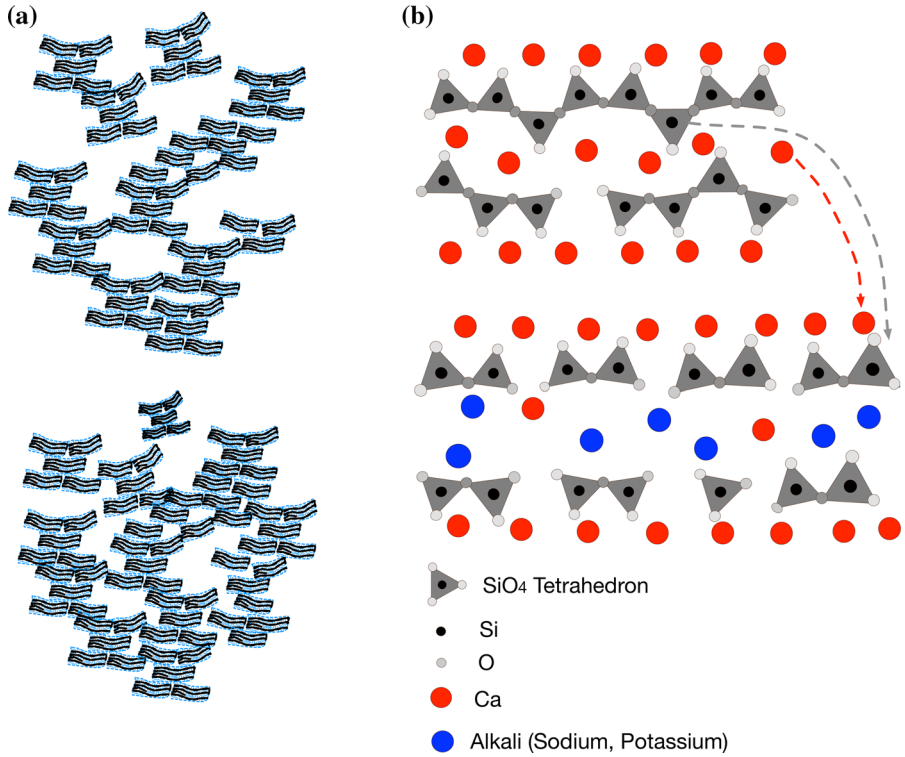

Fig. 6 Schematic illustrations of the effects of alkalis on the **a** packing of C–S–H nanoparticles, **b** atomic structure of C–S–H. The bottom figures show the case for alkali-enriched C–S–H, which has a relatively denser packing density and more disconnected silicate network, in comparison to alkali-free C–S–H shown above

cation (e.g. Na^+, K^+) can potentially serve as an electrostatic attractor and increases the packing density of C–S–H nanoparticles, as illustrated in Fig. 6a [22]. Furthermore, it was confirmed by ^{29}Si nuclear magnetic resonance study that the addition of alkalis reduces the chain length of silicate [28]. It indicates the shortened silicate tetrahedral clusters are easier to re-organize as the network of silicate tetrahedron in alkali-rich C–S–H is more distorted and disconnected [22], in comparison to that in alkali-free C–S–H atomic structure, as illustrated in Fig. 6b.

On the other hand, some researchers [4, 35] claimed that the disjoining pressure is the dominate driving force for shrinkage at high RH range. The disjoining pressure is a distance-dependent pressure characterizing the interaction between two solid surfaces in nano pores. The withdrawal of disjoining pressure in the hindered adsorption layer may result in a reduction of the distance between solid particles, resulting in shrinkage [30]. For OPC containing alkalis, the disjoining pressure can be increased due to the enlarged ionic concentration in the pore water, and therefore the shrinkage magnitude increases [4]. Nevertheless, the present study suggests that the amount of alkalis bound in the solid phases is more important in controlling shrinkage performance of OPC containing alkalis, rather than the free alkalis remaining in the pore solution. For instance, the shrinkage magnitude of NaCl-blended OPC is less than the half of that of NaOH-blended OPC, although the amount of free Na remaining in pore solution is higher, as shown in Table 2.

3.4 Carbonation shrinkage

As illustrated in Fig. 3, for plain OPC system, the carbonation results in higher shrinkage magnitude, which is undoubtedly attributed to the carbonation shrinkage. However, carbonation expansion, rather than shrinkage, is observed for OPC containing sodium salts. Furthermore, carbonation results in similar shrinkage magnitude, but slightly slower kinetics for OPC containing KOH.

As shown in Fig. 3c, the carbonation of OPC results in an *apparent* visco-elastic/visco-plastic characteristic, which shows that the shrinkage magnitude

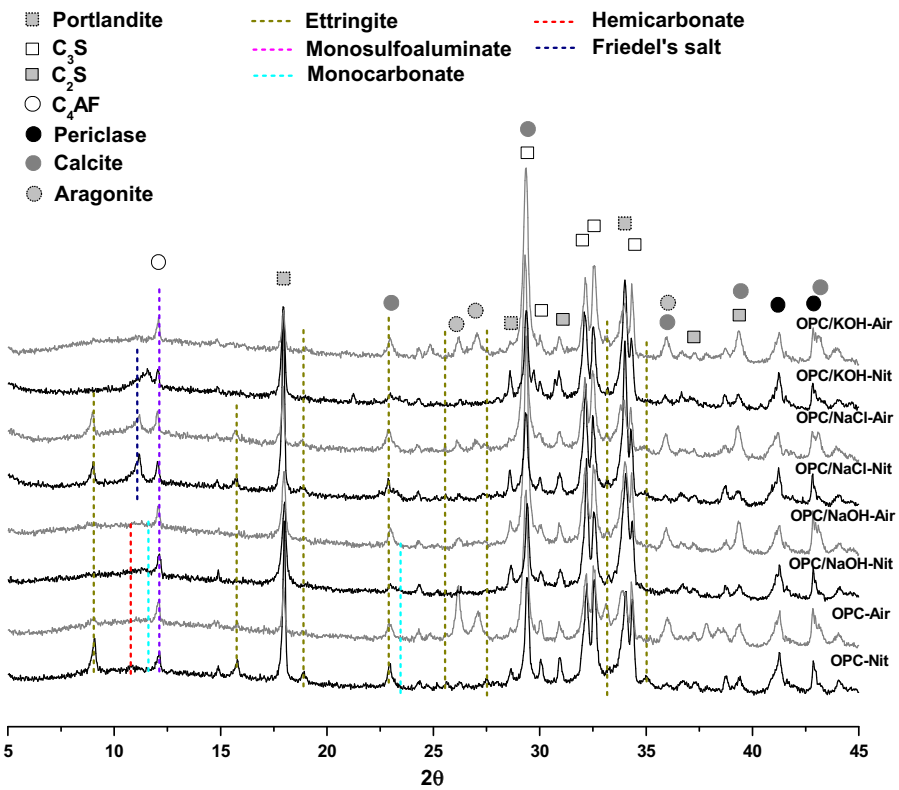

Fig. 7 Comparison of XRD patterns of OPC containing various alkalis dried at nitrogen and atmospheric conditions

continues to increase at constant mass change. However, this almost constant mass does not mean the specimens had reached equilibrium. As shown in Fig. 3b, for OPC dried in air, the mass change undergoes an initial reduction with subsequent gain. Theoretically, the carbonation of portlandite should release 1 mol of water (18 g) per mole of carbon dioxide (44 g) reacted; therefore the carbonation of OPC results in a mass gain. As illustrated in Fig. 5, the samples dried in the air show coarser pore structures than the same mixtures dried in the nitrogen, regardless whether alkali-enriched or not. The pore coarsening can be attributed to the alternation of microstructure due to carbonation, as well as microcracking due to crystallization stress. Although the coarsening of pore structure may result in a reduction in the degree of saturation, the mass change data actually show that the OPC dried in air loses relatively lower amount of mass and tends to gain mass as carbonation proceeds, in comparison to OPC dried in nitrogen. The proceeding carbonation of OPC can also result in a reduction of pH in pore solution, although a residue of portlandite exists [43]. Furthermore, it is impossible to distinguish here whether the carbonation-released water evaporates or is physically adsorbed on the pore wall due to the carbonation-induced modification of water adsorption capability of solid phases. Nevertheless, the competition between carbonation-induced mass gain and the moisture change due to drying, pore coarsening, and modified water adsorption capability results in a misleading phenomenon of equilibrium.

As shown in Fig. 7, carbonation of OPC results in conspicuous dissolution of portlandite and formation of calcite and aragonite. In comparison to plain OPC, the incorporation of alkalis (especially sodium-bearing salts) promotes the formation of calcite rather than aragonite. Theoretically, the formation of calcite due to portlandite carbonation generates 12% volume increase, while the formation of aragonite generates 3% [44]. According to Power's theory [15], the formation of calcium carbonate does not generate volume expansion as it precipices in free pore space which generates little crystallization stress. In agreement with Power's theory, the volume expansion observed in OPC blended with sodium salts can be caused by several reasons. First, the portlandite formed in OPC containing alkalis, especially blended with NaOH, may be in a non-stressed state. As mentioned in Sect. 3.1, the size and morphology of portlandite formed in OPC containing NaOH may be different from that in a plain system, which may be responsible for the extensive generation of more voluminal calcite (rather than aragonite). Secondly, the refined pore structure of OPC containing sodium salts, as shown in Fig. 5, restrains the growth of calcium carbonate crystals, which generates large crystallization stress that generates expansion. Then, the presence of alkalis in pore solution may promote carbonation of pore solution and formation of alkali-rich carbonates. Alternatively, the alkali-rich pore solution in OPC containing alkalis would be more thermodynamically vulnerable to carbonation (i.e. the degree of supersaturation with respect to mixed alkali-calcium carbonates is higher than that of alkali-free calcium carbonates), generating a higher crystallization stress. As a result, this finding proposes that the carbonation-induced volume change in OPC containing alkali salts is not merely determined by the chemical reaction, but also the physical characteristics and pore solution properties of the systems.

4 Conclusions

In this paper, the drying and carbonation shrinkage of OPC containing various alkalis salts were characterized and the mechanisms for the enlarged drying shrinkage, but reduced carbonation shrinkage due to alkali-enrichment were studied. Following conclusions can be drawn based on this study:

1. The incorporation of alkalis in OPC enlarges the magnitude of drying shrinkage but reduces the shrinkage kinetics.
2. The amount of alkalis bound in the solid hydrated phases is more important in controlling the shrinkage performance of OPC, rather than the free alkalis remaining in the pore solution.
3. The enlarged drying shrinkage of OPC due to alkali enrichment can originate from (1) Increased degree of saturation due to refined pore structure and high ionic concentration in pore solution (2) Increased visco-elastic/visco-plastic compliance (i.e. reduced creep modulus) of its solid skeleton due to alkali enrichment.
4. The increased visco-elastic/visco-plastic compliance of alkali-rich OPC is likely due to the alkali

binding in C–S–H, which promotes the packing (rearrangement and reorganization) of C–S–H nanoparticles under drying-induced stresses.
5. The incorporation of alkalis results in carbonation expansion, as compared to the carbonation shrinkage in plain OPC.
6. The volume expansion in OPC containing sodium salts can originate from (1) Formation of more voluminal calcite crystals (rather than the aragonite in plain system); (2) Refined pore structure that restrains the growth of calcium carbonate; (3) Formation of portlandite that is initially in a stress-free status; (4) High degree of supersaturation with respect to alkali-mixed calcium carbonate.

Acknowledgements The authors would like to thank Prof. Farshad Rajabipour for his insightful thoughts and discussion regarding several topics discussed in this paper. The authors gratefully acknowledge the financial support from the US National Science Foundation (NSF) under Award CMMI #1265789. Any opinions, findings and conclusions or recommendations expressed in this material are those of the authors and do not necessarily reflect the views of the NSF.

References

1. Juenger M, Winnefeld F, Provis J, Ideker J (2011) Advances in alternative cementitious binders. Cem Concr Res 41(12):1232–1243
2. Thomas RJ, Ye H, Radlińska A, Peethamparan S (2016) Alkali-activated slag concrete: a closer look at sustainable alternatives to portland cement. Concr Int 38(1):33–38
3. Sant G, Kumar A, Patapy C, Le Saout G, Scrivener K (2012) The influence of sodium and potassium hydroxide on volume changes in cementitious materials. Cem Concr Res 42(11):1447–1455
4. Beltzung F, Wittmann F, Holzer L (2001) Influence of composition of pore solution on drying shrinkage. In: Ulm F-J, Bazant ZP, Wittmann FH (eds) Creep, shrinkage and durability mechanics of concrete and other quasi-brittle materials. Elsevier Science Ltd, Amsterdam
5. Blaine RA (1968) Statistical study of the effects of trace elements on the properties of Portland cement. In: Proc. 5th Int'l symp. chemistry of cement. Tokyo, pp 86–91
6. Beltzung F, Wittmann F, Wan X, Sun W, van Breugel K, Miao C, Ye G, Chen H (2008) Influence of alkali content on creep and shrinkage of cement-based materials. In: International conference on microstructure related durability of cementitious composites. RILEM Publications, pp 905–915
7. Jawed I, Skalny J (1978) Alkalies in cement: a review: II. Effects of alkalies on hydration and performance of Portland cement. Cem Concr Res 8(1):37–51
8. Ye H, Radlińska A (2016) Quantitative analysis of phase assemblage and chemical shrinkage of alkali-activated slag. J Adv Concr Technol 14:245–260
9. Juenger MCG, Jennings HM (2001) Effects of high alkalinity on cement pastes. ACI Mater J 98(3):251–255
10. He Z, Li Z (2005) Influence of alkali on restrained shrinkage behavior of cement-based materials. Cem Concr Res 35(3):457–463
11. Maslehuddin M, Page C, Rasheeduzzafar (1996) Effect of temperature and salt contamination on carbonation of cements. J Mater Civ Eng 8(2):63–69
12. Kobayashi K, Uno Y (1990) Influence of alkali on carbonation of concrete, part 2-influence of alkali in cement on rate of carbonation of concrete. Cem Concr Res 20(4):619–622
13. Neville AM (1995) Properties of concrete, 4th ed. Pearson, Harlow
14. Verbeck GJ (1958) Carbonation of hydrated Portland cement. In: Committee C (ed) Cement and Concrete, STP39460S. ASTM International, West Conshohocken, pp 17–36. https://doi.org/10.1520/STP39460S
15. Powers TC (1900) A hypothesis on carbonation shrinkage, vol 4. Portland Cement Association
16. En Ruiz-Agudo, Kudłacz K, Putnis CV, Putnis A, Rodriguez-Navarro C (2013) Dissolution and carbonation of portlandite [Ca (OH) 2] single crystals. Environ Sci Technol 47(19):11342–11349
17. Chen JJ, Thomas JJ, Jennings HM (2006) Decalcification shrinkage of cement paste. Cem Concr Res 36(5):801–809
18. Matsushita F, Aono Y, Shibata S (2004) Calcium silicate structure and carbonation shrinkage of a tobermorite-based material. Cem Concr Res 34(7):1251–1257
19. Lodeiro IG, Macphee D, Palomo A, Fernández-Jiménez A (2009) Effect of alkalis on fresh C–S–H gels. FTIR analysis. Cem Concr Res 39(3):147–153
20. Mendoza O, Giraldo C, Camargo SS, Tobón JI (2015) Structural and nano-mechanical properties of calcium silicate hydrate (CSH) formed from alite hydration in the presence of sodium and potassium hydroxide. Cem Concr Res 74:88–94
21. Mota B, Matschei T, Scrivener K (2015) The influence of sodium salts and gypsum on alite hydration. Cem Concr Res 75:53–65
22. Ye H, Radlińska A (2016) Shrinkage mechanisms of alkali-activated slag. Cem Concr Res 88:126–135
23. Ye H, Cartwright C, Rajabipour F, Radlińska A (2017) Understanding the drying shrinkage performance of alkali-activated slag mortars. Cement Concr Compos 76:13–24
24. Ye H, Cartwright C, Rajabipour F, Radlińska A (2014) Effect of drying rate on shrinkage of alkali-activated slag cements. In: 4th international conference on the durability of concrete structure (ICDCS). Purdue University, Indiana, pp 254–261
25. Barneyback R, Diamond S (1981) Expression and analysis of pore fluids from hardened cement pastes and mortars. Cem Concr Res 11(2):279–285
26. Glasser F, Kindness A, Stronach S (1999) Stability and solubility relationships in AFm phases: part I. Chloride, sulfate and hydroxide. Cem Concr Res 29(6):861–866
27. Kumar A, Sant G, Patapy C, Gianocca C, Scrivener KL (2012) The influence of sodium and potassium hydroxide on alite hydration: experiments and simulations. Cem Concr Res 42(11):1513–1523

28. Viallis H, Faucon P, Petit J-C, Nonat A (1999) Interaction between salts (NaCl, CsCl) and calcium silicate hydrates (CSH). J Phys Chem B 103(25):5212–5219
29. Lothenbach B, Nonat A (2015) Calcium silicate hydrates: solid and liquid phase composition. Cem Concr Res 78:57–70
30. Ye H, Radlińska A (2016) A review and comparative study of existing shrinkage prediction models for portland and non-portland cementitious materials. Adv Mater Sci Eng 2016(2016):2418219
31. Kovler K, Zhutovsky S (2006) Overview and future trends of shrinkage research. Mater Struct 39(9):827–847
32. Lura P, Jensen OM, van Breugel K (2003) Autogenous shrinkage in high-performance cement paste: an evaluation of basic mechanisms. Cem Concr Res 33(2):223–232
33. Grasley ZC, Leung CK (2011) Desiccation shrinkage of cementitious materials as an aging, poroviscoelastic response. Cem Concr Res 41(1):77–89
34. Badmann R, Stockhausen N, Setzer MJ (1981) The statistical thickness and the chemical potential of adsorbed water films. J Colloid Interface Sci 82(2):534–542
35. Wittmann F (1973) Interaction of hardened cement paste and water. J Am Ceram Soc 56(8):409–415
36. Bentz DP, Garboczi EJ, Quenard DA (1998) Modelling drying shrinkage in reconstructed porous materials: application to porous Vycor glass. Modell Simul Mater Sci Eng 6(3):211
37. Mackenzie J (1950) The elastic constants of a solid containing spherical holes. Proc Phys Soc Lond Sect B 63(1):2
38. Bentz DP (2005) Curing with shrinkage-reducing admixtures. Concrete Int Detroit 27(10):55
39. Vlahinić I, Jennings HM, Thomas JJ (2009) A constitutive model for drying of a partially saturated porous material. Mech Mater 41(3):319–328
40. Lura P, Lothenbach B, Miao C, Ye G, Chen H (2010) Influence of pore solution chemistryon shrinkage of cement paste. In: The 50-year teaching and research anniversary of prof sun wei on advances in civil engineering materials, pp 191–200
41. Jennings HM (2000) A model for the microstructure of calcium silicate hydrate in cement paste. Cem Concr Res 30(1):101–116
42. Ye H (2015) Creep mechanisms of calcium–silicate–hydrate: an overview of recent advances and challenges. Int J Concrete Struct Mater 9(4):453–462
43. Thiery M, Villain G, Dangla P, Platret G (2007) Investigation of the carbonation front shape on cementitious materials: effects of the chemical kinetics. Cem Concr Res 37(7):1047–1058
44. Houst Y (1989) Le retrait de carbonatation. Chantiers (Suisse) 20 (LTP-ARTICLE-2008-036):55-60